ACS APPLIED MATERIALS & INTERFACES

Research Article

www.acsami.org

Synthesis of Nanograined ZnO Nanowires and Their Enhanced Gas Sensing Properties

Sunghoon Park, Soyeon An, Hyunsung Ko, Changhyun Jin, and Chongmu Lee*

Department of Materials Science and Engineering, Inha University, 253 Yonghyun-dong, Nam-gu, Incheon 402-751, Republic of Korea

Supporting Information

ABSTRACT: Polycrystalline ZnO nanowires with grain sizes ranging from 20 to 100 nm were synthesized using a newly designed two-step process: (first step) synthesis of ZnSe nanowires by vapor transportation of a mixture of ZnSe powders; and (second step) thermal oxidation of the ZnSe nanowires at 650 °C. Compared to the single-crystal ZnO nanowire gas sensors and other nanomaterial gas sensors reported previously, the multiple networked nanowire gas sensors fabricated from the nanograined ZnO nanowires showed substantially enhanced electrical responses to NO_2 gas at 300 °C. The NO_2 gas sensing properties of the nanograined ZnO nanowires increased dramatically with increasing NO_2 concentration. The multiple-networked nanograined ZnO nanowire sensor showed a response value of 237,263% at 10 ppm NO_2 and 300 °C, whereas the single-crystal ZnO nanowire sensors showed a response of only 6.5% under the same conditions. The recovery time of the nanograined ZnO nanowire sensor was much shorter than that of the normal ZnO nanowire sensor over the NO_2 concentration range of 1−10 ppm, even though the response time of the former was somewhat longer than that of the latter. The origin of the enhanced NO_2 gas sensing properties of the nanograined ZnO nanowire sensor is discussed.

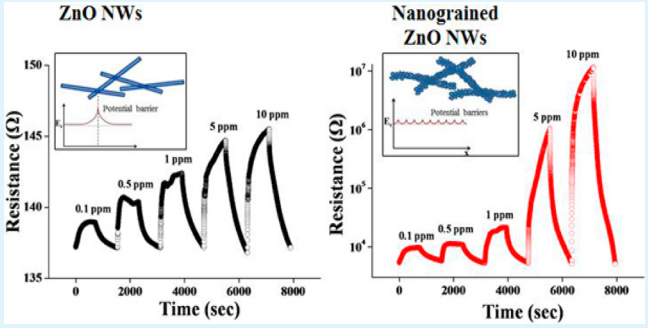

KEYWORDS: *nanowires, ZnO, polycrystalline, Gas sensor, NO_2*

1. INTRODUCTION

In recent years, nanoparticles,[1−4] single-walled carbon nanotubes,[5−9] and semiconducting nanowires[10−14] hold exciting new prospects for application in sensor arrays for the identification and quantification of single or multicomponent chemical and biological agents. Because of their small size, a few molecules are sufficient to change the electrical properties of the sensing elements in electronic transducers.[15] This allows the detection of very low analyte concentrations. In particular, compared to thin film gas sensors, one-dimensional (1D) nanostructure-based sensors have attracted considerable attention because of their higher sensitivity, superior spatial resolution and the rapid response that arises from the high surface-to-volume ratio.[16] Many interesting findings and mechanistic pathways on 1D nanowire gas sensors have been reported recently. For example, the detection of nonpolar analytes with Si nanowire field effect transistors,[17] the critical effect on the hysteresis and surface chemistry on gated silicon nanowire gas sensors,[18] and enhanced sensing of nonpolar volatile organic compounds by silicon nanowire field effect transistors[19] have been reported.

In general, the gas sensing properties of 1D nanostructures depend strongly on the microstructures of nanomaterials as well as on the type of material composing the nanostructures.[20−25] On the other hand, there have been few reports on the effects of microstructures on the sensing properties of 1D nanostructures. Several reports have focused on the enhanced gas sensing properties of nanograined 1D nanostructure gas sensors,[26−28] yet the importance of a nanograined structure in fabricating 1D nanostructure gas sensors should be emphasized further. Also, it is necessary to develop a special technique for the synthesis of nanograined nanowires to produce 1D nanostructured gas sensors with high sensitivity.

On the other hand, NO_2 gas is one of the most dangerous air pollutants. Therefore, the detection of NO_2 gas is of great importance from the viewpoint of both environmental protection and human health. In this study, nanograined ZnO nanowires with grain sizes ranging from 20 to 100 nm were synthesized successfully by the thermal oxidation of ZnSe nanowires. The sensitivity of these ZnO nanowires toward NO_2 gas was compared with that of normal ZnO nanowires, i.e., single-crystal ZnO nanowires.

2. EXPERIMENTAL SECTION

Two different types of ZnO nanowires were prepared: normal ZnO nanowires and nanograined ZnO nanowires. First, normal ZnO nanowires were synthesized on Si substrates by thermal evaporation. Approximately 2 g of a mixture of ZnO and graphite powders (1:1 in

Received: April 27, 2012
Accepted: July 2, 2012
Published: July 2, 2012

weight ratio) as the starting material was placed in an alumina crucible and located at the center of a horizontal quartz tube. A SiO_2/p-type Si (100) substrate coated with an approximately 4 nm thick Au layer was placed downstream inside the tube. The quartz tube was mounted inside a conventional horizontal tube furnace. During nanowire synthesis, the temperature of the quartz tube was maintained at 950 °C for 1 h in an N_2/O_2 atmosphere at N_2 and O_2 flow rates of 500 and 5 sccm, respectively. The pressure in the reactor was kept at 100 Torr. After the synthesis process, the furnace was cooled to room temperature and the Si substrate was removed from the tube.

Nanograined ZnO nanowires were synthesized on SiO_2/Si (100) substrate substrates using a two-step process: (first step) synthesis of ZnSe nanowires by the vapor transportation of a mixture of ZnSe powders; and (second step) thermal oxidation of the ZnSe nanowires. The 300 nm thick SiO_2 thin films were grown on p-type (100) Si and ~4 nm thick Au thin films were deposited on the SiO_2 thin films by direct current (DC) magnetron sputtering. A quartz tube was mounted inside a horizontal tube furnace. The quartz tube consisted of two temperature zones: zone A at 850 °C and zone B at 700 °C. An alumina boat loaded with ZnSe powders and an Au-coated SiO_2/Si substrate were located in zones A and B, respectively. The N_2 gas flow rate was 100 standard cubic centimeters per minute (sccm) and the chamber pressure was 1.0 Torr. The thermal evaporation process for the synthesis of ZnSe nanowires was performed for 1 h. Subsequently, the synthesized ZnSe nanowires were thermally oxidized in an O_2 atmosphere 650 °C for 2 h, which were the optimized oxidation conditions. The oxidation of ZnSe nanowires at temperatures higher than 650 °C would lead to the disintegration of the nanowires due to the evaporation of ZnSe. A shorter oxidation is not able to consume all the Se in the nanowires, resulting in Se impurities in the ZnO nanowires. The Ar gas flow rate and process pressure were 200 sccm and 0.8 Torr, respectively. The collected nanowire samples were characterized by scanning electron microscopy (SEM, Hitachi S-4200) equipped with an energy dispersive X-ray spectrometer (EDXS), transmission electron microscopy (TEM, Philips CM-200), and X-ray diffraction (XRD, Philips X'pert MRD diffractometer).

For the sensing measurements, Ni (~50 nm in thickness) and Au (~100 nm) thin films were deposited sequentially by D. C. magnetron sputtering to form electrodes using an interdigital electrode mask. Multiple networked ZnO nanowire gas sensors were fabricated by pouring a few drops of nanowires-suspended ethanol onto oxidized Si substrates equipped with a pair of IDEs with a gap length of 20 μm. Figure 1 shows a schematic diagram of the multiple-networked ZnO nanowire sensors. The electrical and gas sensing properties of the normal and nanograined ZnO nanowires were measured at 300 °C using a homemade gas sensing measurement system. During the measurements, the nanowire gas sensors were placed in the middle of a sealed quartz tube with a diameter of 50 mm and a length of 800 mm using an electrical feed through. A gas injection tube with a diameter of a quarter inch was located 10 mm away from the sensor. An exhaust line was connected to an end of the quartz tube so that the gas might be exhausted automatically by the difference in pressure between the inside and outside of the tube. A flow-through technique was used to introduce the target air into the system. Controlled amounts of N_2-based 100 ppm NO_2 gas and 99.999% NO_2 gas was injected into the testing tube with a constant flow rate of 500 cc/min using a microsyringe to obtain an NO_2 concentration of 0.1−10 ppm. The electrical resistance of the nanowires was monitored using a Keithley 2612 source meter at 1 V with a sampling rate of resistance of 0.5 s/point. In the case of cleaning, only N_2 gas was introduced with a constant flow rate of 500 cc/min. On the other hand, both the humidity level in the reference air and the level of organic contaminants were not checked in this study.

The response of the ZnO nanowire sensors is defined as $(R_g - R_a)/R_a$ for the oxidizing gas NO_2, where R_a and R_g are the electrical resistances of sensors in air and target gas, respectively. The response time is defined as the time required for the variation in electrical resistance to reach 90% of the equilibrium value after injecting the gas; the recovery time is defined as the time needed for the sensor to return to 90% above the original resistance in air after removing the gas.

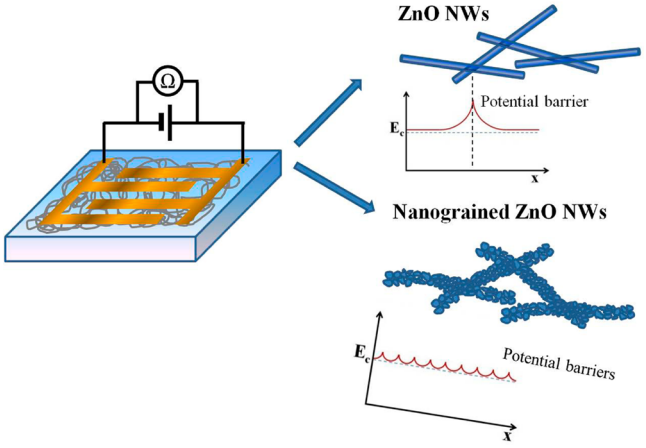

Figure 1. Schematic diagram of a sensor fabricated with normal or nanograined- ZnO nanowires.

3. RESULTS AND DISCUSSION

Figure 2a shows SEM images of the nanograined ZnO 1D nanostructures synthesized by the two-step process newly designed in this study and Figure 2b shows an enlarged SEM image of a typical nanograined ZnO 1D nanostructure. The products were rod-like nanowires with a mean diameter of 400 nm and lengths up to a few hundreds of micrometers. The SEM image of the nanograined ZnO nanowires clearly exhibited very fine grains (Figure 2b). A statistical examination of the SEM images of the as-synthesized nanograined ZnO nanowires revealed a grain diameter in the nanowires ranging from 20 to 100 nm. Figure 2c shows that the nanowire contains no inland grains. In other words, one side of each grain forms a part of the nanowire surface, which suggests that ZnO nucleation occurred heterogeneously at the surface of the ZnSe nanowire. The density of the ZnO nuclei at the ZnSe nanowire surface must be very high because the surface is very unstable chemically. The formation of the ZnO nanowires might proceed by the following steps, as shown in Figure 3:

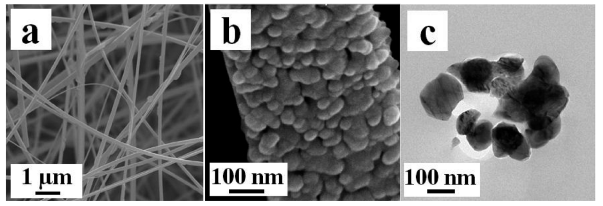

Figure 2. (a) SEM image of nanograined ZnO nanowires, (b) enlarged SEM image of a typical nanograined ZnO nanowire, and (c) TEM image of the cross-section of a typical nanograined ZnO nanowire.

(1) Oxygen absorption, spontaneous oxidation of ZnSe as in the following equation:

$$2ZnSe(s) + O_2(g) = 2ZnO(s) + 2Se(g)$$
$$\Delta G_{f,923K} = -473.38\ KJ/mol \quad (1)$$

and selenium desorption ($\Delta G_{f,923K}$ value is from ref 29);

(2) Formation of ZnO nuclei;

(3) Growth and impingement of the ZnO nuclei;

(4) Coalescence of the ZnO nuclei.

dx.doi.org/10.1021/am300741r | ACS Appl. Mater. Interfaces 2012, 4, 3650−3656

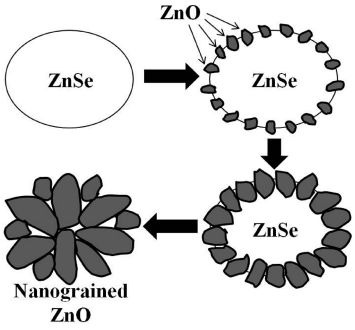

Figure 3. Schematic diagrams of the processes involved in the growth of ZnO nanowires by thermal oxidation of ZnSe nanowires. The figure shows a cross-section of a nanowire changing from ZnSe to ZnO during the oxidation process.

Consequently, polycrystalline ZnO nanowire structures with nanosized grains were obtained by the thermal oxidation process. XPS measurements (Figure 4a–c) confirmed that

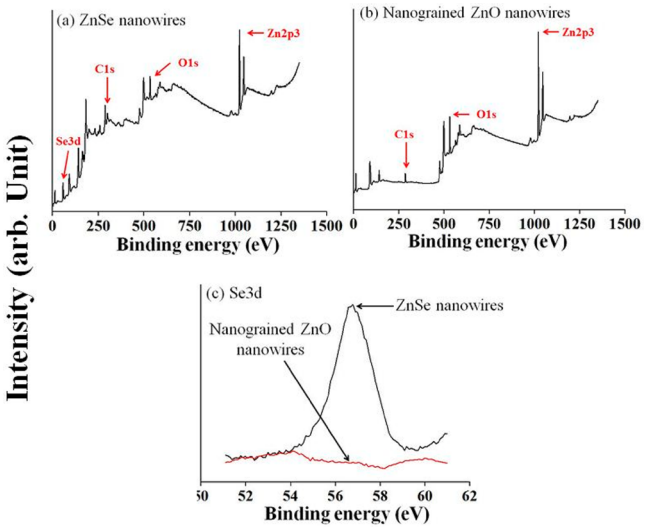

Figure 4. XPS spectra of ZnSe nanowires (a) before oxidation and (b) after oxidation (namely, nanograined ZnO nanowires). (c) Comparison of the XPS Se_{3d} peak intensity of ZnSe nanowires between before and after oxidation.

ZnSe had been completely removed from NWs after oxidation. Figure 4c shows clearly that the ZnSe nanowires do have an XPS Se_{3d} peak whereas the nanograined ZnO nanowires do not (see the Supporting Information). Figure 5 shows XRD patterns of the normal and nanograined ZnO nanowires. The XRD pattern of the single crystal ZnO nanowires showed a particularly high (002) reflection peak and several very low reflection peaks, suggesting that most of the normal nanowires were oriented to (002), which is the preferred orientation of hexagonal-structured ZnO. In contrast, the XRD pattern of the nanograined ZnO nanowires showed several high intensity reflection peaks along with the highest (002) peak, confirming that the nanograined ZnO nanowires are polycrystalline materials, the individual grains of which have various crystallographic orientations of wurtzite-type hexagonal-structured ZnO.

TEM was used for further structural analysis. Figure 6a provides a low-magnification TEM image of a typical nanograined ZnO nanowire. The mean grain size of the

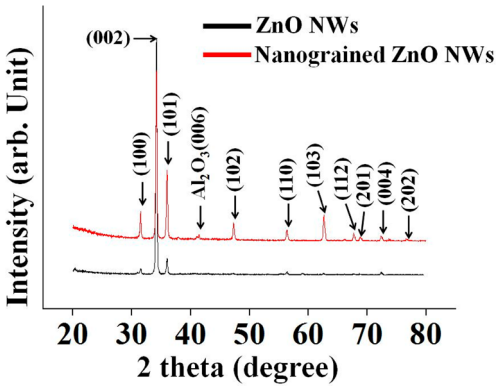

Figure 5. XRD patterns of normal and nanograined ZnO nanowires.

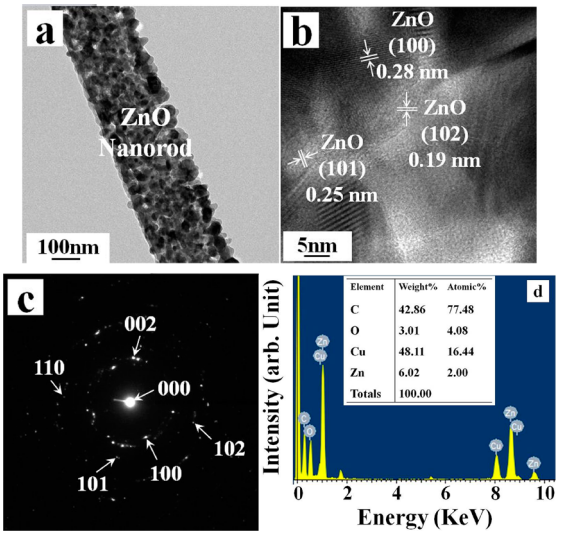

Figure 6. (a) Low-magnification TEM image of a typical nanograined ZnO nanowire, (b) HRTEM image of a typical nanograined ZnO nanowire, (c) corresponding SAED pattern, and (d) EDX spectrum of nanograined ZnO nanowires.

nanograined ZnO nanowire was approximately 60 nm. Images b and c in Figure 6 present a local high-resolution TEM (HRTEM) image and corresponding selected area electron diffraction (SAED) pattern of the nanograined ZnO nanowire, respectively. The HRTEM image with the SAED pattern of the nanograined ZnO nanowires is in good agreement with the nanowire XRD patterns. Local fringe patterns with different orientations were observed. The interplanar spacings of the two neighboring parallel fringes shown in Figure 4b were 0.28, 0.25, and 0.19 nm, which were assigned to the interplanar spacings of the (100), (101), and (102) planes of wurtzite-structured ZnO, respectively. The concentric circle pattern in the SAED pattern indicates that the nanograined ZnO nanowires are polycrystalline. EDXS (Figure 6d) showed that the atomic ratio of O to Zn was approximately 2.04, indicating the nanograined ZnO nanowire to be oxygen-rich. This is in contrast with ZnO thin films synthesized by MOCVD or sputtering, which are commonly Zn-rich. The Cu and C peaks in the EDX spectra are due to the TEM grid.

On the other hand, no grain boundaries were observed in the low-magnification TEM image of a typical normal ZnO nanowire (Figure 7a). The fringe pattern in the HRTEM image (Figure 7b) and the spotty pattern in the SAED pattern

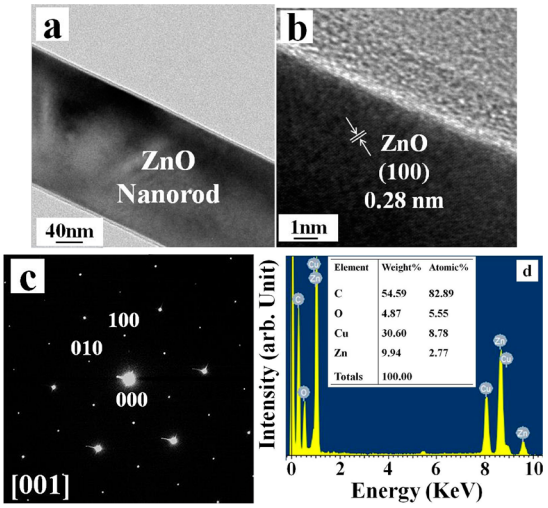

Figure 7. (a) Low-magnification TEM image of a typical normal ZnO nanowire, (b) HRTEM image of a typical normal ZnO nanowire, (c) corresponding SAED pattern, and (d) EDX spectrum of normal ZnO nanowires.

(Figure 7c) indicate that the normal ZnO nanowire was a single crystal. EDXS showed that the O to Zn atomic ratio in the normal ZnO nanowire was approximately 2.00 (Figure 6d). A comparison of the EDX spectra of the normal ZnO nanowire (Figure 7d) with that of the nanograined ZnO nanowires A comparison of Figures 6d and 7d revealed almost no difference in the composition of ZnO between the two different types of ZnO nanowires, even though there was a large difference in the synthesis method between the two types of ZnO nanowires.

Figure 8 presents the PL spectra of the normal and nanograined ZnO nanowires. The intensity ratio of the near-

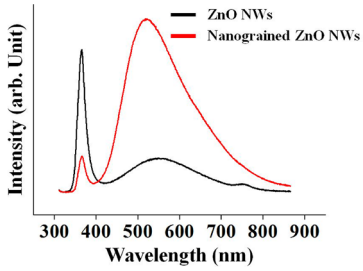

Figure 8. Photoluminescence spectra of normal and nanograined ZnO nanowires.

band edge (NBE) emission to deep level (DL) emission (I_{NBE}/I_{DL}) for the nanograined ZnO nanowires was obviously lower than that of the normal ZnO nanowires, suggesting that nanograined ZnO nanowires are not favorable for use in the fabrication of light emitting devices. ZnO is one of few materials that can emit short wavelength light. Short wavelength light emission is favorable for information storage capacity. Short-wavelength ultraviolet light sources can also find applications in fields such as white light-emitting diode (LED) illumination, sterilization, air purification, and biosensors.[30] Although nanograined ZnO nanowires have inferior PL properties, they appear to be favored for sensor applications, as will be shown later.

Figures 9a and 9c show the dynamic responses of the normal and nanograined ZnO nanowires, respectively, to a typical oxidizing gas NO_2 at 300 °C. The resistance increased upon exposure to NO_2 gas, and recovered completely to the initial value after the removal of NO_2 gas. The sensor responses to NO_2 gas were quite stable and reproducible for the repeated test cycles. Panels b and d in Figure 9 respectively show an enlarged part of the data in panels a and c in Figure 9 measured at 10 ppm NO_2 for normal and nanograined ZnO nanowires to reveal the moments of gas input and gas stop. The normal ZnO nanowires showed responses of approximately 1.4, 2.5, 3.8, 5.6, and 6.5% at 0.1, 0.5, 1, 5, and 10 ppm NO_2, respectively. In contrast, the nanograined ZnO nanowires showed responses of 102, 121, 343, 20 044, and 237 263% at the same NO_2 concentrations, respectively (Table 1). Therefore, the responses of the nanowires were improved approximately 74, 49, 89, 3605, and 36 785 fold at 0.1, 0.5, 1, 5, and 10 ppm NO_2, respectively, by changing their structure from monocrystalline to polycrystalline. In particular, the response of the nanograined ZnO nanowires tended to increase dramatically with increasing NO_2 concentration. This trend of the nanograined ZnO nanowires is in remarkable contrast to that of the normal ZnO nanowires, the response of which was realatively unchanged with increasing NO_2 concentration. In short, the responses of the nanograined nanowire sensors fabricated in this study ranged from approximately 100 to 237 000% at 0.1−10 ppm NO_2. As can be seen in the data listed in Table 2, these responses to NO_2 gas were superior to those of other material 1D nanostructures reported previously.[31−41] The nanograined ZnO nanowires synthesized in this study showed a much higher response than that of other material 1D nanostructures. This substantial enhancement in the response was attributed to the considerably smaller grain size of the nanograined ZnO nanowires. The following two conclusions can be extracted from the above results: (1) polycrystalline ZnO is more favorable than monocrystalline ZnO for NO_2 gas sensing; and (2) the grain size of the 1D nanostructures has a larger effect on the response of the nanostructures than does the type of material composing the nanostructures. In addition to the remarkable sensing responses, the nanograined ZnO nanowire sensor showed recovery times considerably shorter than those of the normal ZnO nanowire sensor over the NO_2 concentration range of 1−10 ppm, even though the response time of the former was somewhat longer than that of the latter, regardless of the NO_2 concentration.

The NO_2 gas sensing mechanism of normal ZnO (n-type semiconductor) nanowires can be depicted as follows. Upon exposure to NO_2 gas, the NO_2 gas is adsorbed by the ZnO nanowires and electrons are released from the ZnO nanowires and attracted to the adsorbed NO_2 molecules because an oxidizing gas such as NO_2 acts as an electron acceptor as shown in the following reactions[42]

$$NO_2(g) + e^- \leftrightarrow NO_2^-(ads) \quad (2)$$

$$NO_2(g) + e^- \leftrightarrow NO(g) + O^-(ads) \quad (3)$$

As a result of these reactions, a depletion layer is created at the surface region of each ZnO nanowire, resulting in an increase in the resistance of the nanowire sensor. On the other hand, when the supply of NO_2 gas is stopped, trapped electrons are released to the ZnO nanowires by NO_2 gas, leading to a decrease in the depletion layer width and resistance. This leads to an increase in carrier concentration in the ZnO nanowires and a decrease in the surface depletion layer width. In other words, the removed electrons are returned to the conduction band, which results in

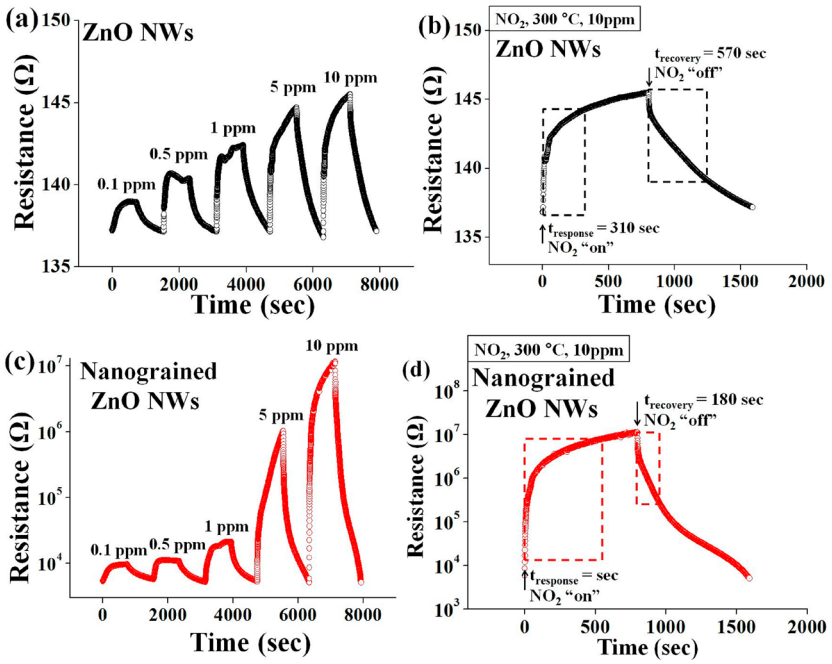

Figure 9. (a) Dynamic response of normal ZnO nanowires. (b) Enlarged parts of the dynamic response curve shown in a at a NO_2 concentration of 10 ppm drawn to reveal the moments of gas input and gas stop. (c) Dynamic response of nanograined ZnO nanowires. (d) Enlarged parts of the dynamic response curve in c at an NO_2 concentration of 10 ppm drawn to reveal the moments of gas input and gas stop.

Table 1. Comparison of the Sensing Properties toward NO_2 Gas between Normal and Nanograined ZnO Nanowires at Various NO_2 Concentrations

	response (%)		response time (s)		recovery time (s)	
NO_2 conc. (ppm)	ZnO	nanograined ZnO	ZnO	nanograined ZnO	ZnO	nanograined ZnO
0.1	1.38 ± 0.1	102.35 ± 10.2	280 ± 28	310 ± 31	450 ± 45	560 ± 56
0.5	2.45	120.96	90	150	390	420
1	3.84	342.76	170	390	500	330
5	5.56	20 044.00	370	630	490	70
10	6.45	237 262.67	310	570	510	180

Table 2. Comparison of the NO_2 Gas Sensing Response of the Different Nanomaterials

nanomaterial	NO_2 conc. (ppm)	response (%)	ref
nanograined ZnO nanowires	0.1	102 ± 10.2	present work
nanograined ZnO nanowires	10	237 263 ± 23 726	present work
ZnO nanorods	0.1	40	31
ZnO powders	0.4	50	32
In-doped SnO_2 nanobelts	0.3	230	33
SnO_2 nanoribbons	3	116	34
SnO_2 hollow spheres	5	1150	35
In_2O_3 nanowires	0.5	35	36
In_2O_3 nanowires	1	3	37
WO_3 microspheres	1	200	38
Au-doped WO_3 powders	10	400	39
SnO_2-core/ZnO-shell nanofibers	70−2000	320	40
$ZnGa_2O_4$-core/ZnO-shell nanowires	10	2500	41

a sharp decrease in the electrical resistance in the ZnO nanowire sensors.

The shapes of the sensing signals might propose diffusion-limited processes. The diffusion-reaction model[43] is that based upon a gaseous substance diffusing through the porous semiconductor layer which can be locally immobilized at a rate much faster than the diffusion process. In a porous thin film, a gaseous substance diffuses and is chemisorbed at grain boundaries. Intragrain diffusion is neglected because it is negligible when compared with the porous nature in the porous thin film. Consequently, the immobility sites are uniformly distributed across the film on pore surfaces. This kind of diffusion-reaction model commonly applies to porous thin films such as sintered oxide semiconductors, yet generally it does not apply to the nanowires synthesized using a common method such as thermal evaporation. However, it might be possible that the nanograined ZnO nanowires contain some micropores because they were prepared using a particular method, i.e., using ZnSe nanowire templates and removing the template by thermal oxidation after the growth of ZnO crystallites. A close examination of the SEM and TEM images indeed revealed the existence of some pores in the nanostructures.

As shown schematically in Figure 1, considerably more electrical barriers are built up at the grain boundaries in nanograined ZnO nanowires because of the smaller grain size, namely, larger grain boundary area than in the normal ZnO nanowires during the adsorption or desorption of gaseous

dx.doi.org/10.1021/am300741r | ACS Appl. Mater. Interfaces 2012, 4, 3650−3656

species. Another thing to consider regarding the number of energy barriers is the intersection of nanowires. The average size of the ZnO grains in the nanograined nanowires is similar to the diameter of the normal nanowires. Under these circumstances, the intersection between two nanograined nanowires would result in many more energy barriers than the intersection between two normal nanowires (where each energy barrier is a result of intersection of two equivalent sizes of ZnO crystallites). Panels a and b in Figure 10 show the intersection of nanograined nanowires and that of normal nanowires, respectively. No grain boundaries are seen at all near the intersection of the normal nanowires (Figure 10b), whereas grain boundaries are observed near the intersection of the nanograined nanowires (Figure 10a), even though the resolution is not good enough. The work function values measured by KP-AFM were 5.049 and 3.279 eV for the nanograined and normal ZnO nanowires, respectively, which also supports that the former has a higher energy barrier at the grain boundary assuming that the differences in electron affinity and electrostatic potential between the two kinds of nanowires are negligible. These potential barriers might serve as resistors in series. A larger number of potential barriers or higher energy barriers would produce a more pronounced change in the electrical resistance in a certain gas environment, resulting in a superior response or sensitivity.[44]

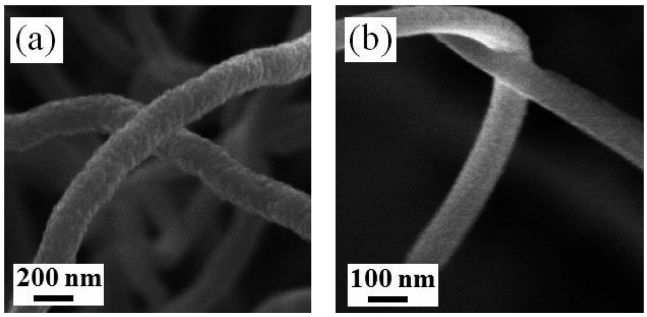

Figure 10. SEM images showing the intersection of (a) nanograined ZnO nanowires and (b) that of normal ZnO nanowires.

BET analysis was carried out in order to investigate the effect of the different processing steps on the specific surface area. The measured specific surface area of the nanograined ZnO nanowires was 16.18 m^2/g as compared to that of the normal grained ZnO nanowires which exhibited almost 5-fold higher specific surface area of 3.17 m^2/g (see the Supporting Information). Thus, a combination of the larger surface area and the larger number of junctions between crossed nanowires might have led the nanograined ZnO nanowires to exceptionally high gas sensitivity. Another thing to consider is the difference in surface coverage between two kinds of nanowires. The nanograined nanowires must have better surface coverage, namely, show lower surface roughness than the normal nanowires. The better surface coverage or the lower surface roughness would make positive effects on the sensitivity of the sensor to gas presumably due to the larger grain boundary areas acting as energy barriers for carrier transport, the larger surface-to-volume ratio, and smaller optical band gap energy. Suchea et al.[45] reported that ZnO films with smaller grains exhibited better sensitivity to ozone due to their larger surface-to-volume ratio and smaller optical band gap energy. The grains in the nanograined nanowires are as long as the radius of the nanowires and aligned along the radial direction. This kind of microstructure may make positive effects on the sensing properties because gas molecules can move more easily to the central region of the nanowire through the grain boundaries aligned in the radial direction and carriers can also move more easily to the central region of the nanowire in the radial direction through the channels or interstitial sites in the ZnO lattice.The other possible explanation is that the grain boundaries can act as preferential diffusion paths for NO_2 gas diffusion. Gas adsorption and desorption might be enhanced in nanograined ZnO nanowires due to the larger grain boundary area per volume, resulting in enhanced sensitivity to gas.

4. CONCLUSIONS

Nanograined ZnO nanowires can be fabricated by the thermal oxidation of ZnSe nanowires. The nanowires fabricated in this study contained no inland grains, presumably because ZnO nucleation occurred heterogeneously at the surface of ZnSe nanowire. Compared to single crystal ZnO nanowire sensors and other nanomaterial sensors reported previously, Multiple-networked ZnO nanowire gas sensors prepared from nanograined ZnO nanowires showed substantially higher electrical responses to NO_2 gas at 300 °C. In addition, the recovery time of the nanograined ZnO nanowire sensor was far shorter than that of the normal ZnO nanowire sensor, even though the response times of the former were somewhat longer than those of the latter. Considerably more electrical barriers were built up at the grain boundaries in the nanograined ZnO nanowires compared to the normal ZnO nanowires during the adsorption or desorption of gaseous species. These potential barriers might serve as resistors in series. The larger number of potential barriers would produce a more pronounced change in electrical resistance in a certain gas environment, resulting in a superior response or sensitivity. We believe that the nanograined ZnO nanowires grown by the method in this study could be used as semiconducting or optical light-emitting devices in nanoscale electronics and electro-optical applications as well as gas sensors at lower production costs.

■ ASSOCIATED CONTENT

Ⓢ Supporting Information

XPS spectra of nanograined ZnO nanowires and BET raw data of nanograined ZnO nanowires. This material is available free of charge via the Internet at http://pubs.acs.org.

■ AUTHOR INFORMATION

Corresponding Author

*Tel.: +82 32 860 7536. Fax: +82 32 862 5546. E-mail: cmlee@inha.ac.kr.

Notes

The authors declare no competing financial interest.

■ ACKNOWLEDGMENTS

This study was supported financially by the Korean Research Foundation (KRF) through the 2010 Core Research Program.

■ REFERENCES

(1) Franke, M. E.; Koplin, T. J.; Simon, U. *Small* **2006**, *2*, 36.
(2) Gouma, P. I.; Prasad, A. K.; Iyer, K. K. *Nanotechnology* **2006**, *17*, S48.
(3) Chen, P. C.; Ishikawa, F. N.; Chang, H. K.; Ryu, K.; Zhou, C. *Nanotechnology* **2009**, *20*, 125503.

(4) Wang, C.; Yin, L.; Zhang, L.; Xiang, D.; Gao, R. *Sensors* **2010**, *10*, 2088.
(5) Kauffman, D. R.; Star, A. *Angew. Chem., Int. Ed.* **2008**, *47*, 6550.
(6) Peng, G.; Trock, E.; Haick, H. *Nano Lett.* **2008**, *8*, 3631.
(7) Peng, G.; Tisch, U.; Haick, H. *Nano Lett.* **2009**, *9*, 1362.
(8) Haick, H.; Hakim, M.; Patrascu, M.; Levenberg, C.; Shehada, N.; Nakhoul, F.; Abassi, Z. *ACS Nano* **2009**, *3*, 1258.
(9) Zilberman, Y.; Tisch, U.; Shuster, G.; Pisula, W.; Feng, X.; Müllen, K.; Haick, H. *Adv. Mater.* **2010**, *22*, 4317.
(10) Patolsky, F.; Timko, B. P.; Zheng, G.; Lieber, C. M. *MRS Bull.* **2007**, *32*, 142.
(11) Cui, Y.; Wei, Q.; Park, H.; Lieber, C. M. *Science* **2001**, *293*, 1289.
(12) McAlpine, M. C.; Ahmad, H.; Wang, D.; Heath, J. R. *Nat. Mater.* **2007**, *6*, 379.
(13) Assad, O.; Haick, H. *IEEE ISIE* **2008**, 2040.
(14) Santra, S.; Guha, P. K.; Ali, S. Z.; Hiralal, P.; Unalan, H. E.; Covington, J. A.; Amaratunga, G. A. J.; Milne, W. I.; Gardner, J. W.; Udrea., F. *Sens. Actuators B* **2010**, *146*, 559.
(15) Tisch, U.; Haick, H. *Mater. Bull* **2010**, *35*, 797.
(16) Mai, L.; Xu, L.; Gao, Q.; Han, C.; Hu, B.; Pi, Y. *Nano Lett.* **2010**, *10*, 2604.
(17) Paska, Y.; Stelzner, T.; Assad, O.; Tisch, U.; Christiansen, S.; Haick, H. *ACS Nano* **2012**, *6*, 335.
(18) Paska, Y.; Haick, H. *ACS Appl. Mater. Interfaces* **2012**, *4*, 2604.
(19) Paska, Y.; Stelzner, T.; Christiansen, S.; Haick, H. *ACS Nano* **2011**, *5*, 5620.
(20) Park, S.; Mackenzie, J. *Thin Solid Films* **1996**, *274*, 154.
(21) Qin, Y.; Shen, W.; Li, X.; Hu, M. *Sens. Actuators B* **1997**, *155*, 646.
(22) Yoon, D.; Choi, G. *Sens. Actuators B* **1997**, *45*, 251.
(23) Zhang, H.; Zhu, Q.; Zhang, Y.; Wang, Y.; Zhao, L.; Yu, B. *Adv. Funct. Mater.* **2007**, *17*, 2766.
(24) Horrillo, M.; Serventi, A.; Rickerby, D.; Gutierrez, J. *Sens. Actuators B* **1999**, *58*, 474.
(25) Kim, I. D.; et al. *Nano Lett.* **2006**, *6*, 2009.
(26) Virji, S.; Huang, J.; Kaner, R. B.; Weiller, B. H. *Nano Lett.* **2004**, *4*, 491.
(27) Gong, J.; Li, Y.; Hu, Z.; Zhou, Z.; Deng, Y. *J. Phys. Chem. C* **2010**, *114*, 9970.
(28) Park, J.; Choi, S.; Kim, S. *Nanotechnology* **2010**, *21*, 475601.
(29) Barin, I. *Thermochemical Data of Pure Substances*, 3rd ed.; VCH: Weinheim, Germany, 1995.
(30) Shur, M.; Gaska, R. *IEEE Trans. Electron. Devices* **2010**, *57*, 12.
(31) Oh, E.; Choi, H. Y.; Jung, S. H.; Cho, S.; Kim, J. C.; Lee, K. H.; Kang, S. W.; Kim, J.; Yun, J. Y.; Jeong, S. H. *Sens. Actuators B* **2009**, *141*, 239.
(32) Baratto, C.; Sberveglieri, G.; Onischuk, A.; Caruso, B.; di Stasio, S. *Sens. Actuators B* **2004**, *100*, 261.
(33) Kaur, J.; Kumar, R.; Bhatnagar, M. C. *Sens. Actuators B* **2007**, *126*, 478.
(34) Law, M.; Kind, H.; Messer, B.; Kim, F.; Yang, P. *Communications* **2002**, *41*, 2405.
(35) Zhang, J.; Wang, S.; Wang, Y.; Wang, Y.; Zhu, B.; Xia, H.; Guo, X.; Zhang, S.; Huang, W.; Wu, S. *Sens. Actuators B* **2009**, *135*, 610.
(36) Vomiero, A.; Bianchi, S.; Comini, E.; Faglia, G.; Ferroni, M.; Sberveglieri, G. *Cryst. Growth Des.* **2007**, *7*, 2500.
(37) Xu, P.; Cheng, Z.; Pan, Q.; Xu, J.; Xiang, Q.; Yu, W.; Chu, Y. *Sens. Actuators B* **2008**, *130*, 802.
(38) Liu, Z.; Miyauchi, M.; Yamazaki, T.; Shen, Y. *Sens. Actuators B* **2009**, *140*, 514.
(39) Xia, H.; Wang, Y.; Kong, F.; Wang, S.; Zhu, B.; Guo, X.; Zhang, J.; Wu, S. *Sens. Actuators B* **2008**, *134*, 133.
(40) Choi, S. W.; Park, J. Y.; Kim, S. S. *Nanotechnology* **2009**, *20*, 465603.
(41) Chen, I. C.; Lin, S. S.; Lin, T. J.; Hsu, C. L.; Hsueh, T. J.; Shieh, T. Y. *Sensors* **2010**, *10*, 3057.
(42) Lin, C.; Chen, S.; Cheng, S.; Lee, H. *Appl. Phys. Lett.* **2004**, *84*, 5040.
(43) Gardner, J. W. *Semicond. Sci. Technol.* **1989**, *4*, 345.
(44) Schierbaum, K.; Weimar, U.; Göpel, W.; Kowalkowski, R. *Sens. Actautors B* **1991**, *3*, 205.
(45) Suchea, M.; Christoulakis, S.; Moschovis, K.; Katsarakis, N.; Kiriakidis, G. *Thin Solid Films* **2006**, *515*, 551.